Microstructure Determination of AOT + Phenol Organogels Utilizing Small-Angle X-ray Scattering and Atomic Force Microscopy

Blake A. Simmons,[†] Chad E. Taylor,[‡] Forrest A. Landis,[§] Vijay T. John,*[,†,||] Gary L. McPherson,*[,‡] Daniel K. Schwartz,[‡] and Robert Moore[§]

Contribution from the Department of Chemical Engineering, Department of Chemistry, Tulane University, New Orleans, Louisiana 70118, and Department of Polymer Science, University of Southern Mississippi, Hattiesburg, Mississippi 39401

Received October 26, 2000

Abstract: Dry reverse micelles of the anionic twin-tailed surfactant bis(2-ethylhexyl) sulfosuccinate (AOT) dissolved in nonpolar solvents spontaneously form an organogel when *p*-chlorophenol is added in a 1:1 AOT:phenol molar ratio. The solvents used were benzene, toluene, *m*-xylene, 2,2,4-trimethylpentane (isooctane), decane, dodecane, tetradecane, hexadecane, and 2,6,10,14-tetramethylpentadecane (TMPD). The proposed microstructure of the gel is based on strands of stacked phenols linked to AOT through hydrogen bonding. Small-angle X-ray scattering (SAXS) spectra of the organogels suggest a characteristic length scale for these phenol−AOT strands that is independent of concentration but dependent on the chemical nature of the nonpolar solvent used. Correlation lengths determined from the SAXS spectra indicate that the strands self-assemble into fibers. Direct visualization of the gel in its native state is accomplished by using tapping mode atomic force microscopy (AFM). It is shown that these organogels consist of fiber bundle assemblies. The SAXS and AFM data reinforce the theory of a molecular architecture consisting of three length scales−AOT/phenolic strands (ca. 2 nm in diameter) that self-assemble into fibers (ca. 10 nm in diameter), which then aggregate into fiber bundles (ca. 20−100 nm in diameter) and form the organogel.

Introduction

Gels constitute an important class of materials due to their applications in templated materials synthesis,[1,2] drug delivery,[3] separations,[4] and biomimetics.[5] In contrast to polymer gels, the gelation of solvents by small molecules is a consequence of self-assembly into networks where physical interactions mediate cross-links and chain entanglements. Several examples of nonpolymeric gelators in the literature include steroids,[6] organometallic complexes,[7] alkylamide derivatives,[8] and fatty acids.[9] The gelation of nonpolar organic solvents with small molecule gelators leads to an interesting class of materials where self-assembly is through molecular interactions that are not electrostatic in nature, but rather a consequence of hydrogen bonding or dispersion interactions. Some recent examples of such systems include the gels of nonpolar solvents with long-chain alkanes reported by Weiss and co-workers,[10] the organogels formed by networks of cholesterol linkages with anthracene derivatives also studied by Weiss and co-workers,[11] the cholesterol−azobenzene linkage based gels of Shinkai and co-workers,[12] and the cholesterol−stilbene and cholesterol−squaraine based gels reported by Whitten and co-workers.[13,14] The gellike system formed by rod-shaped reverse micelles reported by Neuman and co-workers,[15] and Schelly and co-workers[16] also form a relevant class of materials.

We have previously reported that a class of organogels is formed when substituted phenolic compounds, such as *p*-chlorophenol (shown in Figure 1b), are added to anhydrous solutions of the anionic twin-tailed surfactant bis(2-ethylhexyl) sodium sulfosuccinate (AOT, shown in Figure 1a) and a nonpolar solvent.[17−19] These organogels are most stable when

[†] Department of Chemical Engineering, Tulane University.
[‡] Department of Chemistry, Tulane University.
[§] University of Southern Mississippi.
[||] E-mail: vijay.john@tulane.edu. Phone: (504)865-5883. Fax: (504)-865-6744.

(1) Rees, G. D.; Robinson, B. H. *Adv. Mater.* **1993**, *5*, 608.
(2) Loos, M.; Esch, J.; Stokroos, I.; Kellogg, R. M.; Feringa, B. L. *J. Am. Chem. Soc.* **1997**, *119*, 12675.
(3) Haering, G.; Luisi P. L. *J. Phys. Chem.* **1986**, *90*, 5892.
(4) Phillips, R. J.; Deen, W. M.; Brady, J. F. *J. Colloid Interface Sci.* **1990**, *139*, 363.
(5) Hafkamp, R. J. H.; Kokke, P. A.; Danke, I. M.; Guerts, H. P. M.; Rowan, A. E.; Feiters, M. C.; Nolte, R. J. M. *Chem. Commun.* **1997**, 545.
(6) Terech, P.; Ramasseul, R.; Volino, F. *J. Phys. Fr.* **1985**, *46*, 895.
(7) Terech, P.; Chachaty, C.; Gaillard, J.; Giroud-Godquin, A. M. *J. Phys. Fr.* **1987**, *48*, 663.
(8) Hanabusa, K.; Tange, J.; Taguchi, Y.; Koyama, T.; Shirai, H. *J. Chem. Soc., Chem. Commun.* **1993**, 390.
(9) Tachibana, T.; Mori, T.; Hori, K. *Bull. Chem. Soc. Jpn* **1980**, *53*, 1714.
(10) Abdallah, D. J.; Weiss, R. G. *Adv. Mater.* **2000**, *12*, 1237. Abdallah, D. J.; Weiss, R. G. *Langmuir* **2000**, *16*, 352.
(11) Lin, Y. C.; Kachar, B.; Weiss, R. G. *J. Am. Chem. Soc.* **1989**, *111*, 5542. Terech, P.; Furman, I.; Weiss, R. G. *J. Phys. Chem.* **1995**, *99*, 9558. Terech, P.; Ostuni, E.; Weiss, R. G. *J. Phys. Chem.* **1996**, *100*, 3759.
(12) Murata, K.; Aoki, M.; Suzuki, T.; Harada, T.; Kawabata, H.; Komori, T.; Ohseto, F.; Ueda, K.; Shinkai, S. *J. Am. Chem. Soc.* **1994**, *116*, 6664.
(13) Geiger, C.; Stanescu, M.; Chen, L.; Whitten, D. G. *Langmuir* **1999**, *15*, 2241. Wang, R.; Geiger, C.; Chen, L.; Swanson, B.; Whitten, D. G. *J. Am. Chem. Soc.* **2000**, *122*, 2399.
(14) Duncan, D.; Whitten, D. G. *Langmuir* **2000**, *16*, 6445.
(15) Yu, Z.-J.; Zhou, N.-F.; Neuman, R. D. *Langmuir* **1992**, *114*, 5475. Yu, Z.-J.; Neuman, R. D. *Langmuir* **1994**, *10*, 2553.
(16) Feng, K.-I.; Schelly, Z. A. *J. Phys. Chem.* **1995**, *99*, 17207. Feng, K.-I.; Schelly, Z. A. *J. Phys. Chem.* **1995**, *99*, 17212.
(17) Xu, X.; Ayyagari, M.; Tata, M.; John, V. T.; McPherson, G. L. *J. Phys. Chem.* **1993**, *97*, 11350.
(18) Tata, M.; John, V. T.; Waguespack, Y. Y.; McPherson, G. L. *J. Am. Chem. Soc.* **1994**, *116*, 9464.
(19) Tata, M.; John, V. T.; Waguespack, Y. Y.; McPherson, G. L. *J. Phys. Chem.* **1994**, *98*, 3809.

10.1021/ja0037926 CCC: $20.00
Published on Web 02/10/2001

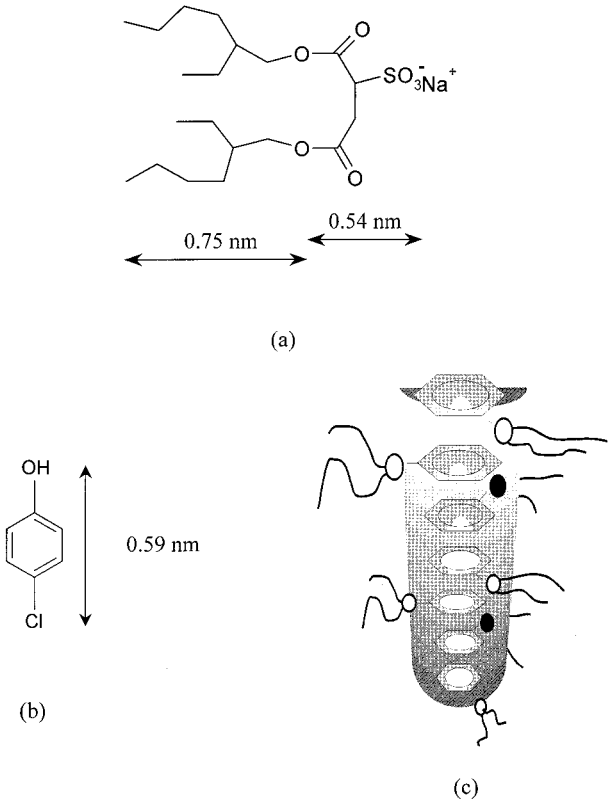

Figure 1. Chemical structures and molecular lengths of (a) bis(2-ethylhexyl) sulfosuccinate (AOT) and (b) *p*-chlorophenol and (c) schematic of the proposed gel structure. The phenolic molecules are stacked to form a strand with the surfactant molecules hydrogen-bonded on the outer surface to form a hydrophilic shell.

the phenol:AOT molar ratio is unity. Typically, AOT in nonpolar solvents typically forms spherical inverse micelles. Upon addition of the phenolic component, the low viscosity micellar solution spontaneously transforms into a rigid organogel. The organogel can be formed at concentrations as low as 3 mM, depending on the choice of nonpolar solvent and phenolic compound used to synthesize the organogel. Gels with para-substituted phenols form efficiently, while ortho-substituted phenols do not form gels. The strength of the organogel, as indicated by its melting point, increases with the pK_a value of the phenolic component.[18,19] The organogels have a sharp melting point and also break down over a period of time when exposed to moisture. Since the gels can be formed can be formed by adding the phenolic component to spherical AOT inverse micelles, it is therefore possible to encapsulate materials (e.g., magnetic and semiconductor nanoparticles) into AOT micelles and then transform the system into encapsulate-containing organogels. Thus, the gels may have applications in the development of new field-responsive materials. Understanding the microstructure of the gels and the nature of the self-assembly is the objective of this paper.

Our previous studies using FTIR spectroscopy have indicated that hydrogen-bonding interactions between the phenol and the sulfosuccinate headgroup of AOT appear to be the driving forces for gelation.[17,19] Furthermore, NMR studies reveal the interesting observation that in the gel state there is a dramatic line broadening of the phenol resonances, while the AOT resonances retain sharp features. The line broadening of the phenol resonances imply that the phenol preferentially becomes motionally restricted on the NMR time scale.[19] Based primarily on the NMR results, we had earlier proposed that the gel strands consisted of stacked phenols with the AOT molecules attached to the external surface of these stacks, with the surfactant tail groups protruding into the bulk solvent.[18,19] Figure 1c illustrates the proposed structure with the stacking of the phenols imposing rigidity to the aromatic species.

In the current study, we provide further evidence of the microstructure of these organogels using tapping mode atomic force microscopy (AFM) and small-angle X-ray scattering (SAXS). SAXS has been used effectively to determine the microstructure of several different molecular systems, including surfactant-based microemulsions,[20,21] polymer gels,[22] and organogels.[23,24] SAXS is a powerful investigative tool in elucidating long-range structures and is especially useful when complemented with other techniques. We show here that tapping mode AFM allows for the direct observation of gel microstructure. Mackie and co-workers employed AFM to observe the interfacial gelation of gelatin.[25] Suzuki et al. utilized AFM to visualize polymer gel surface structure[26] and determined how it is affected by polymer microsphere incorporation into the polymer gel strands.[27] Our work using AFM was motivated by the recent results of Whitten and co-workers who conducted an AFM study investigating gelators containing cholesterol attached to *trans*-stilbene derivatives or squaraine dyes.[13] These gelators were shown to produce a fibrous network throughout the gel mass. We show that a similar fibrous network exists in the phenol + AOT organogels and that the dimensions of this network are a function of the gelator and solvent selection and the gelator concentrations.

Experimental Section

Materials and Sample Preparation. All chemicals were purchased from Aldrich as analytical grade quality reagents and used as received. To remove any trace water from bis(2-ethylhexyl) sulfosuccinnate (AOT), it was dried in a vacuum oven at 80 °C for 4 h before use. Organogels were synthesized by dissolving a measured amount of AOT in the chosen solvent and then adding an equimolar amount of *p*-chlorophenol. The solvents used were benzene, toluene, *m*-xylene, 2,2,4-trimethylpentane (isooctane), decane, dodecane, tetradecane, hexadecane, and 2,6,10,14-tetramethylpentadecane (TMPD). The *p*-chlorophenol does not completely solubilize in the alkane solvents but is completely miscible with the aromatic solvents used. For the alkane mixtures, the presence of the AOT enhances the solubility of the *p*-chlorophenol (through AOT, chlorophenol hydrogen bonding) so that equimolar mixtures can be incorporated into solution to form isotropic gel phases. Typically, pregel mixtures, contained in 20 mL capped vials to prevent water absorption from the ambient air, were heated at 40−70 °C in a warm water bath and sonicated until all components were dissolved as evidenced by a clear isotropic solution. The mixtures were then removed from the water bath and allowed to cool and gelate at room temperature. Upon organogel formation, these systems were extremely rigid and varied from clear (aromatic solvents) to turbid (alkane solvents) in appearance.

Small-Angle X-ray Scattering (SAXS). Samples were prepared by placing a small amount of the gel between two circular Teflon sheets (diameter ~2 cm), compressing them, and then placing them in a sample holder. After SAXS analysis the samples were still in the gel phase, with no visibly observable structural breakdown. SAXS measurements were conducted at the University of Southern Mississippi (Hattiesburg,

(20) Radiman, S.; Toprakcioglu, C.; Faruqi, A. R. *J. Phys. Fr.* **1990**, *51*, 1501.
(21) Barnes, I. S.; Hyde, S. T.; Ninham, B. W.; Derian, P. J.; Drifford, M.; Zemb, T. N. *J. Phys. Chem.* **1988**, *92*, 2286.
(22) Yeh, F.; Sokolov, E. L.; Walter, T.; Chu, B. *Langmuir* **1998**, *14*, 4350.
(23) Terech, P.; Ostuni, E.; Weiss, R. G. *J. Phys. Chem.* **1996**, *100*, 3759.
(24) Terech, P.; Furman, I.; Weiss, R. G. *J. Phys. Chem.* **1995**, *99*, 9558.
(25) Mackie, A. R.; Gunning, A. P.; Ridout, M. J.; Morris, V. J. *Biopolymers* **1998**, *46*, 245.
(26) Kobiki, Y.; Suzuki A. *Int. J. Adhes. Adhes.* **1999**, *19*, 411.
(27) Suzuki, H.; Suzuki A. *Colloids Surf., A* **1999**, *153*, 487.

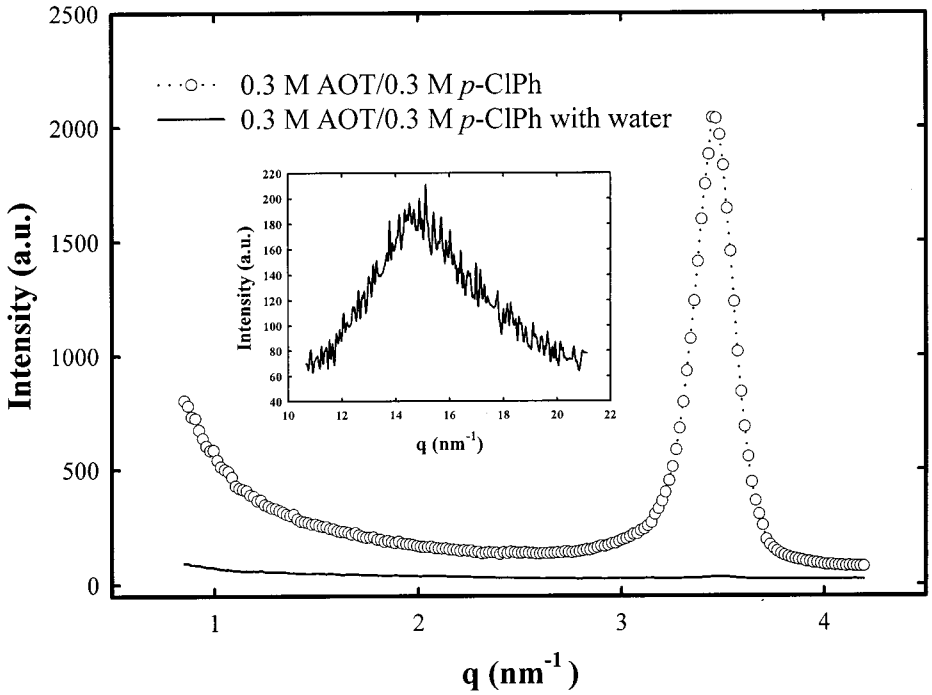

Figure 2. SAXS spectra of a 0.3 M AOT/0.3 M *p*-chlorophenol organogel synthesized in isooctane before and after the addition of water, demonstrating a complete breakdown of the gel microstructure. The water amount used is equivalent to $W_0 = 4$ (= $[H_2O]/[AOT]$). The inset displays the X-ray diffraction spectra of a 0.2 M AOT/0.2 M *p*-chlorophenol organogel synthesized in isooctane.

MS) on a Siemens XPD-700P polymer diffraction system, equipped with a two-dimensional position-sensitive area detector. The sample-to-detector distance was 49 cm. A sealed tube source was used to produce the Cu Kα radiation ($\lambda = 0.154$ nm). Because of instrument limitations, the q range was 0.7−4.2 nm^{-1}. The scattered intensity is presented as a function of the transformed wave vector $q = (4\pi/\lambda)\sin(2\theta/2)$, where 2θ is the scattering angle and λ the Cu Kα radiation wavelength. Spectral analysis and background subtraction was performed with the v2.109 General Area Detector Diffraction System (GADDS) Siemens software package.

X-ray Diffraction (XRD). A Scintag XDS-2000 equipped with a Cu Kα_1 radiation source and a Si (Li) detector was used to record the diffraction data of the organogel. The X-ray tube was operated at 45 kV and 40 mA. A scan rate of 0.64 nm^{-1} min was employed to scan q from 10.7 to 21.1 nm^{-1}.

Atomic Force Microscopy (AFM). Samples analyzed by AFM were prepared by pouring small amounts of the melted organogel into a Petri dish containing a mica disk, which served as the sample substrate. Once pouring was completed, the Petri dish was tightly capped to prevent water absorption by the gel and/or excessive solvent evaporation, and the gel was allowed to set. The gel-coated mica disk was then excised with a scalpel and tweezers from the Petri dish and mounted on a metal puck for subsequent AFM imaging.

The gels were imaged in ambient conditions with a NanoScope III AFM (Multimode SPM, Digital Instruments, Santa Barbara, CA) equipped with an E scanner. All images were acquired in tapping mode using etched silicon probes (Pointprobes, Nanosensors) operated at their fundamental resonance frequencies (ω_o) of 200−235 kHz. These 125 μm long cantilevers had a nominal force constant (k) of 27−53 N/m, a tip radius curvature (r_t) of 5−10 nm, and tip half-angles (θ) of 17° (side), 25° (front), and 10° (back). The tip vibrational frequency was set on the low frequency side of the resonance peak to a value corresponding to a free air tip amplitude of 70% of the resonance peak height amplitude. Height and amplitude mode images were recorded simultaneously at a scan rate of 2.54 Hz and a scan angle of 0°. To minimize sample damage and maintain sustain sufficient tracking of the tip with the gel features, ratio (r_{sp}) values of the engaged or set point tip amplitude (A_{sp}) to its free air amplitude (A_o) ($r_{sp} = A_{sp}/A_o$) were manually maximized.

In height mode imaging, the cantilever deflection amplitude is ideally kept constant throughout a sample (x,y) scan by movement of the sample vertically with respect to the vibrating tip. The vertical position of the sample at each (x,y) data point makes up the topographic/height image. Fine structural features or sharp edges are sometimes not tracked accurately by the feedback electronics; collection of this "error signal" as an amplitude image can reveal details obscured in the height data. The amplitude images do not provide accurate height information about our sample features, yet they do show accurate structural details as a result of sensitive edge detection.

Image processing and analysis was performed with the Nanoscope software package. In particular, images were corrected for sample tilt and bow by performing the Planefit filter and for long wavelength roughness by Fourier 2D filtering. Heights and widths of sample features were measured using the section analysis utility.

Results and Discussion

SAXS. The SAXS spectrum of a 0.3 M AOT/0.3 M *p*-chlorophenol organogel synthesized with 2,2,4-trimethylpentane (isooctane) is shown in Figure 2. The presence of the strong, single peak indicates that a characteristic length scale is present in the organogel, with an associated degree of ordering related to the inverse of the corresponding peak width. The intensity increase present in the low q value region for the organogel is attributed to beam-stop interference. The lack of any secondary or harmonic peaks in the spectra indicates that the organogel has no long-range crystalline order. When water is added to the organogel, the SAXS peak is observed to disappear (Figure 2). The water amount used to break the organogel is equivalent to $W_0 = 4$ ($W_0 = [H_2O]/[AOT]$). This is due to the disruption of the hydrogen bonds between the hydroxyl groups of the phenolic molecules and the carbonyls of the AOT. Once these bonds are disrupted the organogel quickly loses its molecular architecture, the gel phase is lost, and the system becomes a single-phase low viscosity liquid solution. An organogel sample is observed to liquefy within 30 s after this trace amount of water is added.[17,18] The inset to Figure 2 displays the X-ray diffraction (XRD) spectrum for a 0.2 M AOT/0.2 M *p*-chlorophenol organogel synthesized with isooctane over the q range of 10.7 to 21.1 nm^{-1}. There is a

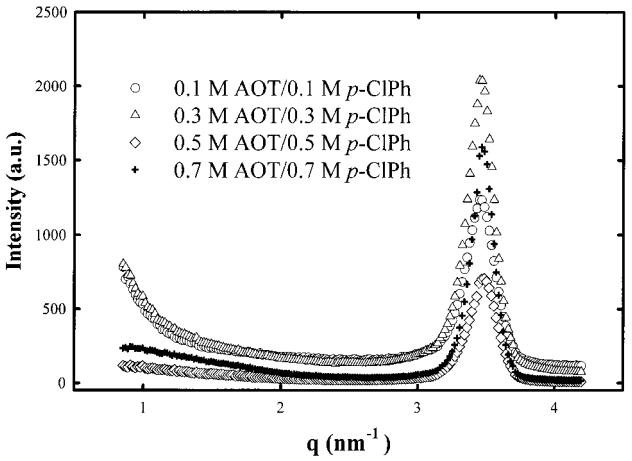

Figure 3. SAXS spectra of organogels synthesized in isooctane at different equimolar AOT + *p*-chlorophenol concentrations.

Table 1. SAXS q Values (q_m), d Spacings (d_m), and Correlation Lengths (ξ) of Phenolic Organogels Synthesized with Isooctane

[AOT] and [*p*-ClPH]	q_m (nm^{-1})	d_m (nm)	ξ (nm)
0.1	3.45	1.82	6.21
0.3	3.45	1.82	8.47
0.5	3.48	1.80	9.17
0.7	3.47	1.81	11.49

broad peak that has a maximum at a q value of 14.7 nm^{-1}, corresponding to a d spacing of 0.43 nm. This feature could be due to the phenol stacks that would exist in the proposed molecular architecture. The broadness of the peak implies that the stacking of the phenols does not have long-range order. The fact that there are no other peaks than at these two regions in the X-ray spectra indicates that the neighboring stacks are also arranged in a random fashion in relation to each other throughout the organogel.

Figure 3 displays the SAXS spectra of the AOT/*p*-chlorophenol/isooctane organogels at different concentrations. There is no systematic trend of peak intensity with concentration. Table 1 lists the q values associated with the maximum peak intensities (q_m), the respective Bragg d spacings at these q_m values ($d_m = 2\pi/q_m$), and the corresponding correlation lengths (ξ) obtained from a Lorentzian three-parameter model fit of the data. The correlation lengths (increasing from 6.2 to 11.5 nm with increasing concentration) suggest that the individual organogel strands are aggregated into specific domains. The observed increase in the correlation length ξ with increasing phenol and AOT concentration may be indicative of enhanced domain aggregation during the gelation process.

The q_m values are relatively constant at a value of ca. 3.5 nm^{-1} for these organogels. This indicates that they share the same fundamental building block for their microstructure, regardless of the surfactant/phenol concentration. The corresponding d spacing of the q_m value is ca. 1.8 nm. If it is assumed that the strands self-assemble in the close-packed hexagonal arrangement for cylinders, as shown in Figures 4a and 4b, the radius ($r = d/\sqrt{3}$ for that geometry) of each strand would be 1.05 nm. Molecular schematics (HyperChem Lite v1.1, Hypercube, Inc., Gainesville, FL) give lengths of the *p*-chlorophenol and AOT molecules to be 0.59 and 1.29 nm, respectively, with the AOT headgroup being 0.54 nm long and the remainder, 0.75 nm, assigned to the alkyl tails (the alkyl tails are assumed to be in the fully extended conformation). Dependent upon the degree of tail overlap present in neighboring AOT molecules, a minimum and a maximum radius (Figure 4c) can be calculated

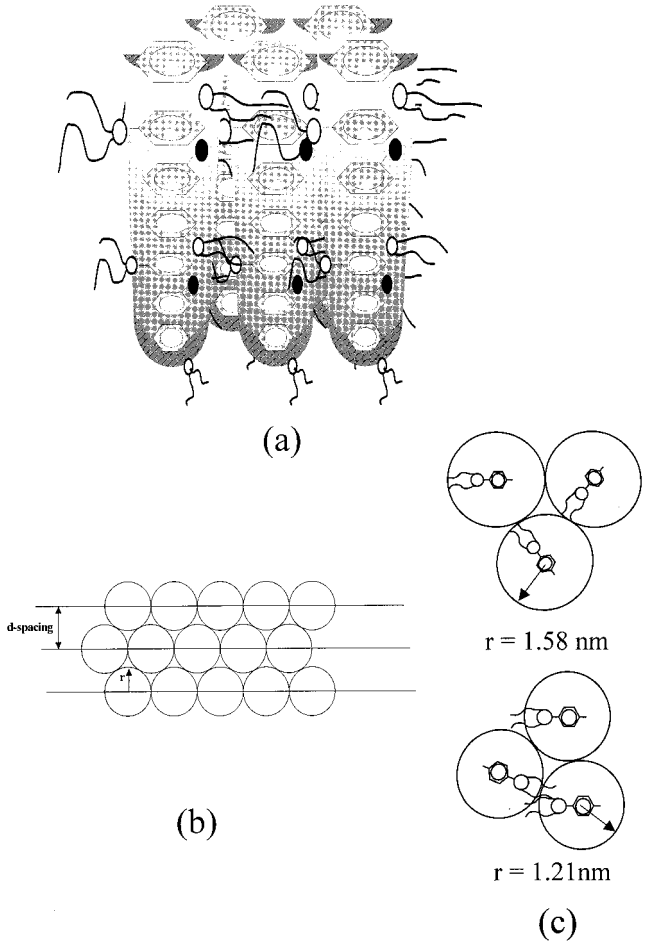

Figure 4. (a) Schematic of strand aggregation to fibers. (b) Cross-section of the fiber illustrating the basic repeat unit as seen by SAXS. (c) Schematic depicting packing modes of AOT + phenol to form the fibers. The top image represents the AOT arrangement without tail overlap, while the bottom image represents the AOT arrangement with tail overlap between neighboring strands.

from the molecular modeling results and compared with the SAXS data. The maximum calculated strand radius occurs when the AOT tails have no overlap between them (the repeat distance, or diameter, would therefore consist of 2 AOT molecules and a *p*-chlorophenol molecule) and would be 1.58 nm. The minimum calculated strand radius, with complete tail overlap (the repeat distance would be one *p*-chlorophenol molecule, two AOT headgroups and one AOT tail), is 1.21 nm. The SAXS strand radius of 1.05 nm obtained for the organogels synthesized with isooctane is below the minimum calculated from the modeling results, indicating that the tail configuration of the AOT as it exists in the organogels may not be fully extended, as was assumed. Additionally, the hydrogen bonding between the C═O groups of AOT and the phenol hydroxyl group would result in a degree of headgroup overlap, which would again reduce the radius from the end-to-end configuration assumed in the calculation.

Thus, SAXS results are consistent with a hexagonal close-packing of the individual strands, resulting in fibers of aggregated strands. The strand radius calculated through the d spacing is relatively close to that calculated from molecular dimensions when the gelators (AOT + *p*-chlorophenol) are arranged in the structure proposed from NMR and FTIR information. The SAXS results add some validity to the strand structure proposed from NMR information and additionally indicate that the strands are themselves aggregated into fibers.

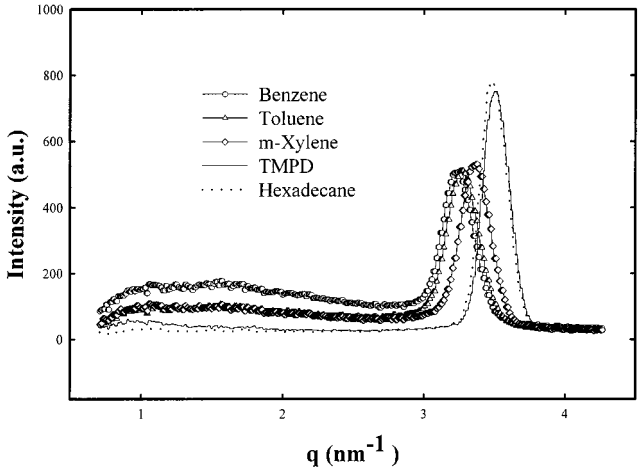

Figure 5. SAXS spectra of 0.2 M AOT/0.2 M *p*-chlorophenol organogel synthesized with different nonpolar solvents.

Table 2. SAXS q Values (q_m), d Spacings (d_m), and Correlation Lengths (ξ) Obtained from 0.2 M AOT/ 0.2 M *p*-Chlorophenol Organogel Synthesized with Different Solvents

solvent	q_m (nm^{-1})	d_m (nm)	ξ (nm)
benzene	3.24	1.94	7.35
toluene	3.28	1.92	7.36
m-xylene	3.38	1.86	7.86
TMPD	3.51	1.79	10.32
hexadecane	3.51	1.79	10.32

The strand aggregation to fibers is the next level of our understanding.

The solvent used to synthesize the organogel influences the position of the peak maximum to a small but measurable level. This effect can be seen in Figure 5, which shows the SAXS spectra of the 0.2 M AOT/0.2 M *p*-chlorophenol organogel system synthesized with different solvents. The q_m and d_m values obtained for these organogels are presented in Table 2. There is a trend in the q values observed in the SAXS spectra that reflects the solvent dependency. The smallest and largest q_m values are present in the organogel synthesized with benzene (3.24 nm^{-1}) and hexadecane (3.51 nm^{-1}), respectively. The use of smaller solvents such as benzene therefore reflects slightly larger d spacings and consequently larger effective strand radii. We attribute this observation to solvent penetration between strands. Constituent groups added to benzene (i.e., toluene and *m*-xylene) lead to a decrease in the effective strand radius. The planarity of the aromatic solvents may add to its ability to be incorporated between gel strands. As the solvent is changed from an aromatic solvent to a straight- or branched-chain alkane, the q_m values increase further. We note that the q_m values for the aliphatic hydrocarbon solvents fall in the narrow range of 3.45 nm^{-1} for isooctane to 3.51 nm^{-1} for hexadecane (Tables 1 and 2). The smaller effective strand radii when these solvents are used indicate that the solvents do not swell the fiber structure to the same degree as the aromatic solvents. The linear and branched chain hydrocarbon solvents, therefore, may not penetrate into the inter-strand regions. There is also a systematic trend present in terms of the correlation lengths obtained from the SAXS data for the aromatic and aliphatic organogels. The smallest correlation lengths (7.35−7.86 nm) are present in those organogels synthesized with the aromatic solvents. The aliphatic organogels produce identical and larger (10.32 nm) correlation lengths. This may be indicative of a change in the aggregation behavior of the strands during the gelation process, with the aromatic organogels having smaller aggregate dimensions of the strands than those of the aliphatic organogels.

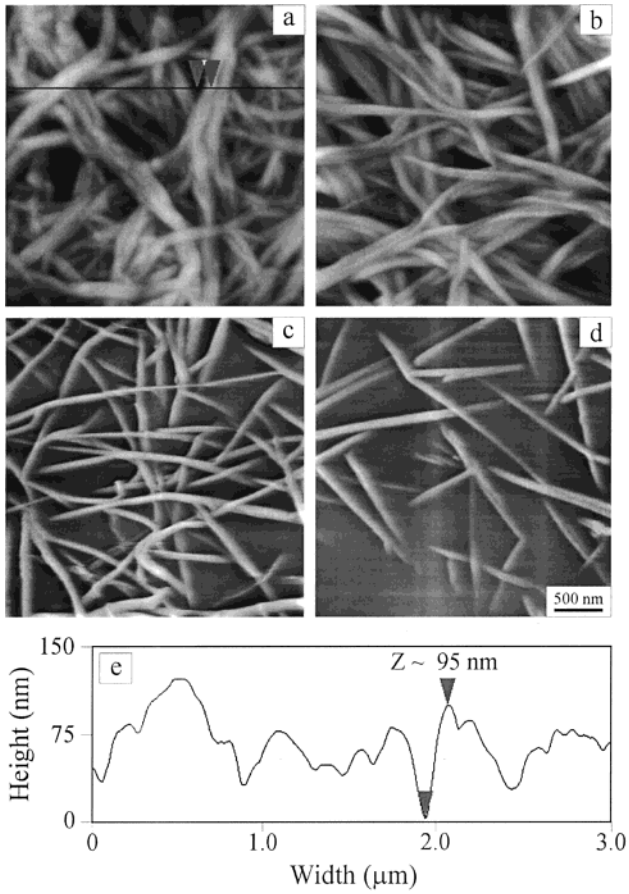

Figure 6. Height AFM images of 0.2 M AOT/0.2 M *p*-chlorophenol organogels in (a) isooctane, (b) decane, (c) tetradecane, and (d) 2,6,10,14-tetramethylpentadecane (TMPD). All images are 3.0 μm × 3.0 μm. Cross-sectional cut of (a) is displayed in (e).

Tapping Mode AFM. To directly observe the microstructure of the organogels and minimize sample damage, tapping mode AFM was performed. Because of difficulties encountered during sample preparation, only those organogels synthesized with the alkane solvents were studied with AFM. Height and amplitude images of these phenolic organogels were recorded simultaneously. Figure 6 illustrates 3 μm × 3 μm height images for 0.2 M *p*-chlorophenol/0.2 M AOT organogels synthesized in (a) isooctane, (b) decane, (c) tetradecane, and (d) 2,6,10,14-tetramethylpentadecane (TMPD). A cross-sectional view of Figure 6a is presented in Figure 6e. In all four gel systems, an extensive fibrous network is observed. The fibrous network is qualitatively similar to those observed in the cholesterol−stilbene system by Whitten and co-workers.[13] The characteristic width of the fibrous features is of the order of 100 nm, significantly larger than the length scales observed through SAXS. Closer examination of these networks indicates, however, that they are made with bundles of fibers. The density of the fibrous network appears to be greater in the isooctane and decane gel systems (Figure 6a and b, respectively) than in the tetradecane and TMPD organogel systems (Figures 6c and d, respectively). This result is attributed to surface solvent loss from the isooctane sample during sample preparation for AFM analysis. The solvent loss is either due to partial evaporation of the lower boiling point solvent or a degree of solvent drainage (syneresis) upon excision of the gel-coated mica disk. The AFM images of the higher boiling solvents, tetradecane and TMPD, may be more representative of the true gel networks (Figures

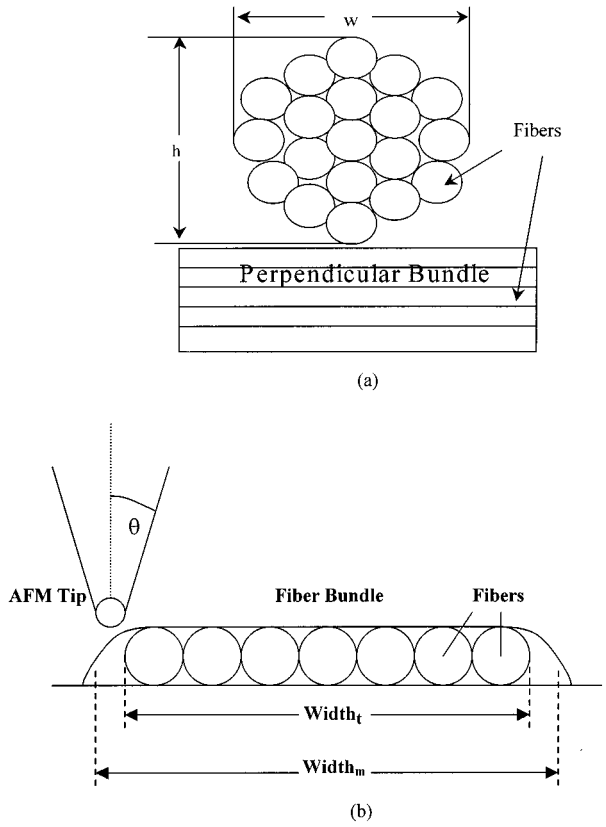

Figure 7. Diagram depicting (a) fiber bundle intersection where height and width measurements are made and (b) interaction of the AFM tip with a fiber bundle.

6c and d, respectively) where fiber bundles are suspended in and dispersed by the immobilized bulk solvent.

These images indicate that the fiber bundles in isooctane are typically broader than those observed in decane, tetradecane, and TMPD. Furthermore, the average fiber bundle width in the latter three solvents appears to be qualitatively similar. Thus, with the exception of isooctane, these images suggest there is no dependence of these widths on solvent chain length. The fact that the shapes and sizes of the fiber bundles in TMPD are qualitatively similar to those of decane and tetradecane indicates that solvent structure (branched-chain or straight-chain paraffins) also has no drastic affect on these gel characteristics. This result directly agrees with the SAXS data presented above.

To get accurate height and width information from the height images, a procedure for data analysis was developed. The strand dimensions were only measured for those strands directly atop an underlying fiber bundle (Figure 7a). This was done in order to provide an accurate base line for the fiber bundle being measured. Reported average fiber bundle widths and heights were acquired by measuring 5−8 fiber bundles per gel system. The exception for this is found in the 0.05 M *p*-chlorophenol/0.05 M AOT organogel synthesized with tetradecane. For this organogel sample, only three fiber bundles were measured due to the small number of fibers exposed atop the gel surface that also met the above condition for measurement. To get accurate widths of the fiber bundles, AFM tip deconvolution was performed using Odin's equations[28] for imaging of a sphere with a conic tip terminated by a spherical apex, the tip geometry of the Si probes used. Gel samples were imaged at a scan angle of 0°, and thus tip half-angle (θ) values of 35° (front) and 0° (back) apply along a scan line, after accounting for tip inclination in the cantilever holder of ca. 10°. A tip half-angle (θ) of 17° and the maximum quoted radius of curvature (r_t) of 10 nm were used in calculation of the true fiber bundle widths. Figure 7b depicts interaction of the tip with a fiber bundle containing individual, cylindrical fibers. This figure also demonstrates the difference in the measured and true fiber bundle widths caused by such tip interaction. Of course, the tip−fiber bundle interaction and the observed enlargement of the true fiber bundle width are dependent on the bundle dimensions. In fact, for a r_t of 10 nm and a θ of 17°, the tip−fiber bundle interaction is that of a cone−sphere type at fiber bundle heights ≥ 11.0 nm. For heights smaller than 11.0 nm, the tip−fiber bundle interaction is that of a sphere−sphere nature.

(28) Odin, C.; Aime, J. P.; Kaakour, El; Bouhacina. *Surf. Sci.* **1994**, *317*, 321.

Table 3. Average Fiber Dimensions of Phenolic Organogels

gel system[a]	height[b] (nm)	width[b] (nm)	width[c] (nm)	width[c]/height
0.2 M/iC$_8$	21.0 ± 8.3	131 ± 31	109 ± 28	5.5 ± 1.3
0.05 M/iC$_8$	8.8 ± 4.1	48 ± 11	31 ± 9	4.1 ± 1.7
0.2 M/C$_{10}$	37.8 ± 24.8	102 ± 42	74 ± 34	2.4 ± 0.9
0.2 M/C$_{12}$	33.6 ± 5.8	103 ± 13	77 ± 11	2.3 ± 0.2
0.2 M/C$_{14}$	33.7 ± 16.0	87 ± 16	60 ± 13	2.1 ± 0.7
0.05 M/C$_{14}$	2.7 ± 0.1	33 ± 4	21 ± 4	7.6 ± 1.4
0.2 M/C$_{16}$	29.8 ± 8.9	91 ± 20	66 ± 18	2.3 ± 0.4
0.2 M/TMPD	32.4 ± 4.9	99 ± 14	73 ± 13	2.2 ± 0.2

[a] The concentrations listed define the equimolar concentrations of AOT and *p*-chlorophenol dissolved in the specific solvent. iC8, TMPD, and C$_n$ are abbreviations for isooctane, 2,6,10,14-tetramethylpentadecane, and straight-chain alkanes of *n* carbons, respectively. [b] Fiber dimensions measured with Nanoscope software. [c] Fiber widths calculated after tip deconvolution.

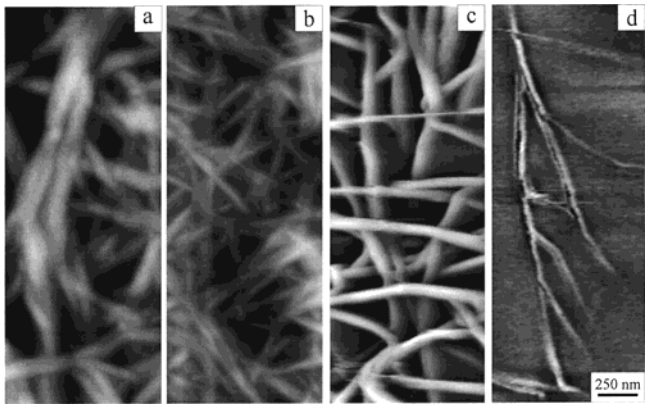

Figure 8. Height AFM images of 0.2 M AOT/0.2 M *p*-chlorophenol organogels in (a) isooctane and (c) tetradecane; 0.05 M AOT/0.05 M *p*-chlorophenol organogels in (b) isooctane and (d) tetradecane. All images are 3.0 μm × 3.0 μm.

Table 3 lists the measured heights, apparent widths, and calculated true widths of the fiber bundles observed in Figure 6 and all the other gel systems analyzed during the course of the current study, utilizing the data analysis procedure discussed in the preceding paragraph. Also included in this table are the calculated width/height ratio values of the fiber bundles. With the exception of the isooctane gel system, the fiber bundles within these organogels have average heights of ca. 30−40 nm and widths of ca. 60−80 nm. The average fiber bundle height and true width of 21.0 ± 8.3 nm and 109 ± 28 nm, respectively, in the isooctane gels is again attributed to partial solvent loss from within the fiber bundles. It is speculated that such solvent loss may act to collapse and deform the fiber bundles into an elliptical or oval shape, such that smaller fiber bundle heights and larger true widths typically result. It is also noted that the fiber bundle widths are consistently larger than their heights, by factors of 5.5 for isooctane and 2.1−2.4 for all the other

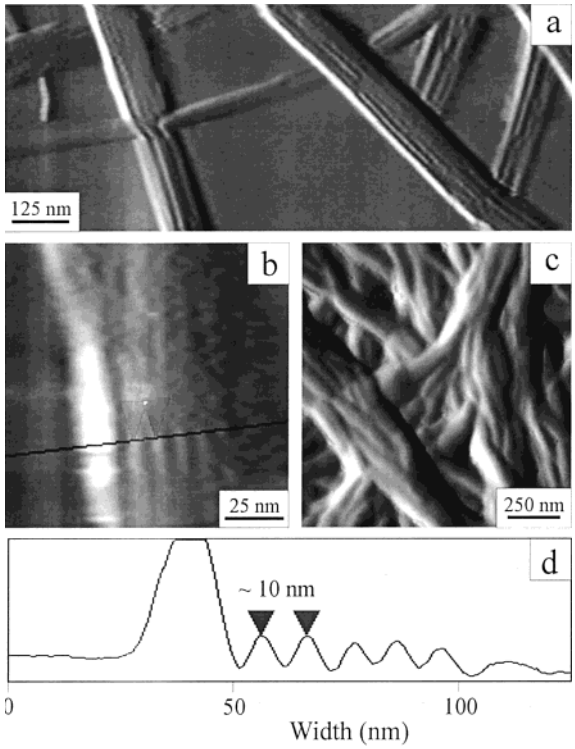

Figure 9. Amplitude AFM images of 0.2 M AOT/0.2 M *p*-chlorophenol organogel in (a) and (b) 2,6,10,14-tetramethylpentadecane (0.5 μm × 1.25 μm and 0.25 μm × 0.25 μm, respectively) and (c) isooctane (1.25 μm × 1.25 μm). Cross-sectional cut of the fiber bundle in (b) is displayed in (d); the smaller internal strands are approximately 10 nm wide.

solvents at the concentration of 0.2 M. In fact, fiber bundle width/height ratio values less than 1 were almost never observed. Although it is not surprising that the organogel fiber bundle structures are not perfectly cylindrical, we would have expected random orientations of these fiber bundles, such that width/height ratio values inverse to those observed would have also been detected and the average ratio would be unity. This would be far outside the uncertainties associated with our tip deconvolution procedure. Also, the observed bundle dimensions were not affected by tip load, suggesting that the apparent anisotropy is not an artifact due to compression or damage during imaging. We conclude that the anisotropy is real and reflects an intrinsic property, such as surface tension, of the gel sample.

Figure 8 demonstrates the effect of decreasing the phenol/AOT concentration from 0.2 to 0.05 M on the dimensions of fiber bundles in isooctane (Figures 8a and 8b) and tetradecane (Figures 8c and 8d). For both organogel systems, these images clearly demonstrate a significant decrease in fiber bundle dimensions with a decrease in the phenol/AOT concentration. The measurements are listed in Table 3 and clearly indicate smaller fiber bundle dimensions at the lower concentration of 0.05 M. Heights and true widths for the 0.05 M isooctane system are 8.8 ± 4.1 nm and 31 ± 9 nm, respectively, and 2.7 ± 0.1 nm and 21 ± 4 nm, respectively, for the 0.05 M tetradecane system. The measured width/height ratio value of 7.6 ± 1.4 for the fiber bundles in tetradecane may be due to slight tip damage/deformation to those selected for measurement. Perhaps some small amount of damage to such thin fiber bundles is unavoidable and possibly accountable for the general increase in the width/height ratio at the lower concentration. In summary, we attribute the smaller fiber bundle dimensions at lower concentrations to a reduction in the aggregation of individual fibers during gelation.

Figure 9 represents our attempts to clearly define the individual fibers in a fiber bundle. Figures 9a and 9b illustrate amplitude images of a 0.2 M organogel synthesized with TMPD. The parallel features running along the length of the fiber bundles pictured in these figures are in fact smaller fibers. Figure 9d displays the cross-sectional profile of the large fiber bundle in Figure 9b. This profile indicates the presence of at least 5 smaller fibers constituting this larger fiber bundle. Significantly, the profile also indicates periodic spacing of these smaller fibers, indicating that they are all approximately 10 nm wide, as shown in Figure 9d. This number is in good agreement with the correlation lengths obtained from the SAXS data presented in Tables 1 and 2, especially the correlation length of 10.32 nm (Table 2) produced by the SAXS of the TMPD organogel. Figure 9c presents a similar observation of intertwined fibers within a fiber bundle for an organogel synthesized with isooctane. The parallel fibers of the gel with TMPD contrast with the intertwined fibers of the gel with isooctane. The parallel fiber structure is intrinsic to the TMPD system, while we are unsure whether the intertwined fiber structure of the isooctane system is a consequence of solvent loss during sample mounting

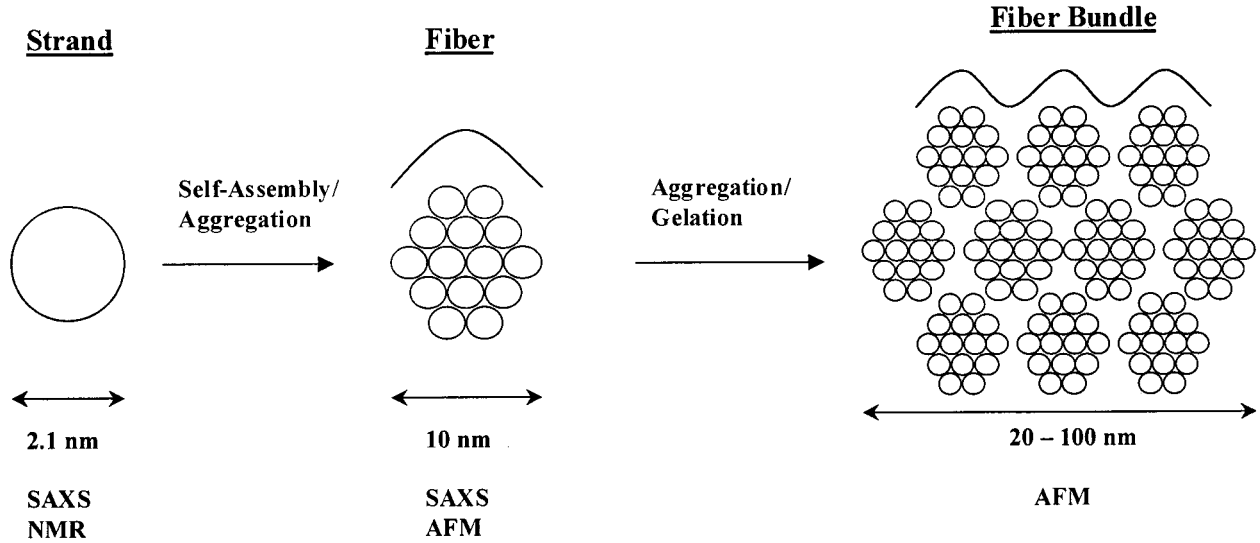

Figure 10. Diagram of the three levels of organization present in the phenolic organogels (strand, fiber, fiber bundle), the length scales of each, and the observational method utilized.

and imaging. Of interest in Figure 9a is also the observation of apparently interpenetrating fiber bundles accompanied by a deflection in the propagation direction of the fibers at the penetration point.

Proposed Organogel Microstructure. SAXS and AFM thus provide complementary information to our earlier NMR results. From the SAXS data and the molecular length scales, a single strand of the molecular architecture depicted in Figure 1c should have a radius in the range of 1.05 nm (diameter 2.1 nm). This would mean that an observed fiber that is approximately 10 nm wide would incorporate about 5 strands in the width dimension, or 14−18 strands total within the fiber volume. These fibers proceed to self-assemble into the observed fiber bundles that form the backbone of the organogel and are clearly observable through AFM. A schematic of these three length scales is presented in Figure 10. The gelation process can therefore be broken into three stages that follow the length scales presented. The first stage is the self-assembly of the phenolic stacks and the hydrogen bonding of the AOT on the exterior to form discrete strands. These strands then aggregate into fibers, perhaps through dispersion interactions between overlapping surfactant tails. The final stage is the further aggregation of these fibers into large fiber bundles. The growth and interpenetration of these fiber bundles leads to a cross-linked network that exerts sufficient capillary force to immobilize the solvent on a macroscopically observable scale.

Conclusions

The microstructure of a novel organogel has been investigated with tapping mode AFM and SAXS. Our previous work with FTIR and NMR characterizations has led to the proposed stacked phenol strand architecture shown in Figure 1c. The information obtained from the SAXS data of the organogels allows us to refine this model to one that involves aggregation of these strands to fibers and enables a correlation of the stacked phenol architecture with molecular length scales. The tapping mode AFM results give us clear evidence of structure on a larger length scale where fibers aggregate to fiber bundles.

Thus, NMR, FTIR, SAXS, XRD, and AFM serve as complementary techniques to characterize the self-assembly of AOT and the phenolic component to a class of novel organogels. In continuing work, we seek to understand the dynamics of such self-assembly in systems when no agitation is provided and the process of gelation is diffusion-controlled. Inverse micelles have significant potential as nanoreactors in the synthesis of inorganic clusters. The transformation of nanoparticle-containing dry micelles to organogels may result in new field responsive gel materials. The potential to examine such particle-containing structures through AFM certainly exists.

Acknowledgment. Support from the National Science Foundation (Grant 9909912) and DARPA (Grant MDA972-97-1-0003) is gratefully acknowledged. C.T. and D.K.S. acknowledge support from the National Science Foundation (Grant 9980250).

JA0037926